Polarization of carbon electron-momentum density in lithium-graphite intercalation compounds

S. Rabii
Department of Electrical Engineering, University of Pennsylvania, Philadelphia, Pennsylvania 19104-6390

J. Chomilier and G. Loupias*
Laboratoire de Minéralogie-Cristallographie, Université Pierre et Marie Curie et Université de Paris VII, 4 place Jussieu, 75252 Paris CEDEX 05, France

(Received 29 December 1988)

Compton-profile measurements on the second-stage lithium-graphite intercalation compound, LiC_{12}, have been performed with the high-resolution spectrometer of Laboratoire pour l'Utilisation du Rayonnement Electromagnétique for two directions, parallel to the c axis and average in the basal plane. Simultaneously, a new *ab initio* self-consistent-field energy-band structure has been calculated for LiC_{12} with the actual stacking of graphite layers. The wave functions have been used to obtain Compton profiles. Both theory and experiment confirm the failure of the rigid-band model for Li-graphite intercalation compounds, as well as the importance of the polarization of graphite valence orbitals due to the presence of lithium ions.

I. INTRODUCTION

Graphite intercalation compounds (GIC's) are synthesized by inserting foreign atoms or molecules (intercalants) between carbon layers in graphite.[1] Since graphite is a semimetal, the electron donated or accepted by the intercalant modifies the electronic properties of graphite and results in metallic behavior of the final material. This process leads to a series of compounds with regular stacking of n graphite layers between two successive intercalant planes; n is referred to as the stage of the compound. In this paper we extend previous theoretical[2,3] and experimental[4,5] studies of electronic-momentum distribution in graphite and first-stage lithium-intercalated graphite, to the second-stage compound. This investigation of the role of lithium in graphite is carried out using Compton scattering.

Among alkali GIC's, lithium compounds exhibit the highest degree of three dimensionality in their electronic properties.[6] The electronic conductivity anisotropy of LiC_6 is of the order of 10^6 in contrast with 10^3 for graphite, while its in-plane conductivity is the highest among the donor compounds.[7] The original (rigid-band) model for the electronic structure of lithium GIC assumed that π bands of graphite remain undistorted by intercalation and the alkali atom simply donates its outer electron to the previously empty antibonding π^* bands of graphite folded into the smaller Brillouin zone of the GIC. From here onward, π and π^* refer to the occupied bonding and unoccupied antibonding π bands in graphite. Direct experimental evidence to support the breakdown of the rigid-band model has been provided by the measurements of Compton profiles in graphite and LiC_6 (Refs. 4 and 5), where one probes the momentum density and thus the detailed nature of wave functions. At the same time, the wave functions obtained by energy-band calculations[8,9] were used to obtain theoretical Compton profiles.[2,3] The excellent agreement between theory and experiment provides a good test for the quality of wave functions and for the non-rigid-band effects. Other energy-band calculations for LiC_6 (Refs. 10–12) have also demonstrated the inapplicability of the rigid-band model to the first-stage lithium GIC.

For the purpose of the present study, we have calculated a new self-consistent energy-band structure for LiC_{12} using the actual $A\alpha AA\alpha A$ stacking[13] (Fig. 1) rather than the hypothetical $A\alpha AB\beta BC\gamma C$ assumed in the previous calculation.[9] AA stacking refers to the case where all the carbon atoms in two successive layers are located directly on top of each other, while in AB stacking (graphite) only one-half of carbon atoms in these two layers are in registry. The Greek letters denote one of a set of distinct sites that could be occupied by the intercalant ions.

Section II describes the samples used in this study. The electronic-momentum density is introduced in Sec. III. Section IV deals with the theoretical and experimental techniques and Sec. V is devoted to the results and discussion. The conclusion is presented in Sec. VI.

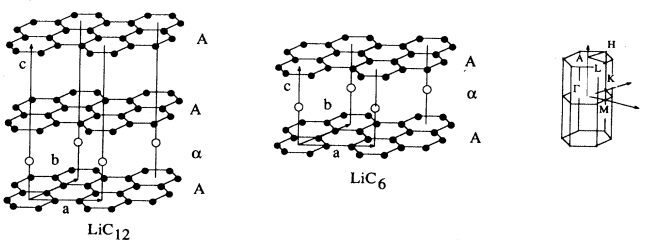

FIG. 1. Stacking sequence of the first- and second-stage lithium GIC: LiC_6 and LiC_{12}. Also shown is the Brillouin zone with high-symmetry points for a hexagonal structure.

II. SAMPLES

Since fairly large samples are needed for Compton measurements (typically 2 cm^3), highly oriented pyrolytic graphite (HOPG) is used in their preparation. HOPG is composed of domains whose **c** axes are parallel to within half a degree, but are randomly oriented with respect to each other in the basal plane. Thus these measurements provide directional profile along the **c** axis but an average profile in the basal plane.

The intercalation is achieved using the two-zone furnace technique, where the temperature gradient between graphite and the alkali metal controls the stage.[14] Since lithium GIC are very reactive, they are kept in sealed cells equipped with two beryllium windows that do not give any contribution to the Compton profile. These cells are filled with dry argon without the presence of nitrogen. Stability of the samples is checked by recording the 001 x-ray reflections. Absence of any change in the sample color during the entire period of the experiment is additional proof that no change of stage is taking place by the deintercalation of lithium. To obtain the required thickness of the sample (typically 5 mm), a set of plates of GIC is placed on top of each other. Thus we are certain of the stoichiometry, even in the center of the sample.

III. ELECTRON-MOMENTUM DISTRIBUTION

When a photon is inelastically scattered by an electron, the momentum and energy conservation laws lead to a relation between the photon energy loss and the projection of the initial electron momentum **p** on the scattering vector **K**. The energy loss ($\hbar\omega$) of these photons is composed of two terms.[15] The first is due to scattering by an electron at rest (the Compton shift) and is related only to the scattering angle. The second is a Doppler broadening around the Compton shift and accounts for the motion of the electrons in the sample.[16] Thus

$$\hbar\omega=\hbar^2K^2/2m+hq/m \ , \tag{1}$$

where $q=\mathbf{K}\cdot\mathbf{p}/K$ and **K** is the scattering vector. Throughout this paper, we will use atomic units (a.u.) for which $h=m=1$.

In a solid, the Doppler broadening component of the energy loss is referred to as the directional Compton profile (DCP) and its amplitude, at a certain q, is equal to the density of the electrons whose momenta have a projection equal to q along **K**:

$$J(q,\mathbf{e})=\int n(\mathbf{p})\delta(\mathbf{p}\cdot\hat{\mathbf{e}}-q)d\mathbf{p} \ , \tag{2}$$

where $\hat{\mathbf{e}}$ is a unit vector parallel to **K** and $n(\mathbf{p})$ is the momentum distribution of the electrons. This relation applies when the requirements for impulse approximation are fulfilled, i.e., for independent electron scattering and when scattering is so fast that the potential seen by the ejected electron is the same in both the initial and final states.[17]

Thus one can map the three-dimensional electronic distribution in momentum space, $n(\mathbf{p})$, by measurement of a set of DCP's. However, since in this case the measurements were not carried out on single crystals, but on materials based on HOPG, we can only obtain an average profile in the basal plane in addition to the profile along the **c** axis.

Since the scattering is incoherent, this technique, which is a bulk probe, is insensitive to crystal defects and can successfully be applied to these compounds. Since valence electrons in solids have a large extent in real space, their resulting localization in momentum space makes them ideal subjects for investigation by Compton scattering. This is particularly appropriate for the present study since we are only interested in the conduction- and valence-band wave functions.

IV. THEORETICAL AND EXPERIMENTAL TECHNIQUES

A. Theory

One can define the wave function in momentum space, $\chi(\mathbf{p})$, such that

$$n(\mathbf{p})=\chi(\mathbf{p})\chi^*(\mathbf{p}) \ . \tag{3}$$

$\chi(\mathbf{p})$ for a specific state is related to the Fourier expansion of the wave function $\psi_{n,\mathbf{k}}(\mathbf{r})$,

$$\psi_{n,\mathbf{k}}(\mathbf{r})=\sum_{\mathbf{G}}C_{n,\mathbf{k}}(\mathbf{G})\exp[i(\mathbf{k}+\mathbf{G})\cdot\mathbf{r}] \ , \tag{4}$$

where n is band index, **k** wave vector in the first Brillouin zone, and **G** a reciprocal-lattice vector. Thus

$$J(q,\mathbf{e})=(1/N)\sum_{n}\sum_{\mathbf{k}}\sum_{\mathbf{G}}|C_{n,\mathbf{k}}(\mathbf{G})|^2\Theta(E_F-E_{n,\mathbf{k}}) \times\delta((\mathbf{k}+\mathbf{G})\cdot\hat{\mathbf{e}}-q) \ , \tag{5}$$

where E_F is the Fermi energy and Θ limits the sum over the bands to the occupied states. N is a normalization factor.[18,19]

The coefficients $C_{n,\mathbf{k}}$ are obtained by carrying out a self-consistent energy-band calculation for LiC_{12} within the Hohenberg-Kohn-Sham density-functional approximation,[20,21] using *ab initio* norm-conserving pseudopotentials[22] and the Hedin-Lundqvist parametrization of the exchange-correlation potential.[23] As mentioned in the Introduction, this new calculation is carried out for the actual structure of LiC_{12}. The basis set used is a mixture of plane waves and localized orbitals.[24] The details of this approach are given elsewhere.[8,9] The final self-consistent wave functions are then expanded entirely in plane waves, obtaining the $C_{n,\mathbf{k}}$'s.

The energy bands are calculated for a uniform grid of 30 **k** points in an irreducible sector of the Brillouin zone (BZ) having a volume equal to $\frac{1}{24}$ of the full hexagonal zone. Since the **c** axis dimension of the unit cell for LiC_{12} is almost twice that of LiC_6, its BZ is about half the volume of the latter. For this reason we expect to obtain the same accuracy as the calculation performed for LiC_6 and graphite[2,3] which used a grid of 45 **k** points. The common list of reciprocal-lattice vectors in the expansion of the wave function at all **k** points contains 2000 reciprocal-lattice vectors. Since the fundamental lattice vector along the **c** axis for LiC_{12} is approximately half of

that for LiC_6, 2000 reciprocal-lattice vectors are not sufficient to allow the c-axis profile to be calculated beyond 3.05 a.u. However, as in the case of graphite and LiC_6, the Compton profile anisotropy reduces to zero beyond 3.0 a.u. Thus we extend the profile in the c direction to 5.0 a.u. by setting it equal to the average basal plane value beyond 3.0 a.u. The average basal plane profile is calculated by dividing the $K-\Gamma-M$ irreducible sector of the BZ into seven segments and calculating the directional profiles for eight angles in this region. The average of these results gives the profile in the basal plane.

The space group of graphite is $P6_3mc$ with lattice parameters $a=2.456$ Å and $c=6.696$ Å. LiC_6 and LiC_{12} have the same space group, $P6/mmc$, with lattice parameters $a=4.305$ and 4.288 Å, and $c=3.706$ and 7.065 Å, respectively.

B. Experiment

The experiments are carried out using a monochromatic beam provided by the synchrotron facility and the focusing high-resolution spectrometer[25] of Laboratoire Pour l'Utilisation du Rayonnement Electromagnétique. The entire energy-loss spectrum of the photons scattered at a specific angle is recorded simultaneously, by means of a Cauchois curved analyzing crystal using Si(400) reflection in the vertical plane. The photons of the same energy, emitted at various points of the sample, are Bragg reflected when going through the analyzing crystal and focused at a single point of the Rowland circle. Each position in the Rowland circle is then related to certain energy by Bragg analysis. A position-sensitive detector, filled with xenon at 3.5 atm pressure, is tangent to this circle and used to record the entire Compton spectrum.

The incident energy used for the experiments is 12 858 eV with a 10-eV bandwidth, and the scattering angle is 137°, resulting in a Compton shift of 540 eV. The theoretical profiles presented here have been convolved with a Gaussian of 0.16 a.u. of momentum width at half maximum. This corresponds to the experimental resolution, including scattering angle accuracy, energy bandwidth, and detector resolution.

The raw data are corrected for all energy-dependent terms, such as absorption, analyzer reflectivity, and detector efficiency. The energy scale is then converted into momentum scale. The positive values of q are chosen to be the low-energy side of the profile. A calculated atomic-core profile is subtracted from the total in order to obtain the valence profile. The resulting profile is then corrected for multiple-scattering contributions, i.e., photons that are scattered more than once, using a Monte Carlo simulation.[26] In order to make comparison with graphite meaningful, the profiles in this study are normalized to the number of electrons per carbon atom. Thus LiC_{12}, LiC_6, and graphite profiles are normalized to $4\frac{1}{12}$, $4\frac{1}{6}$, and 4, respectively.

V. RESULTS AND DISCUSSION

In order to clearly observe the characteristics of the additional electron in the GIC, as well as the modifications in graphite electronic distribution brought about by intercalation, we show the difference between measured profiles of GIC and graphite in Fig. 2 for the scattering vector parallel to the c axis. The difference profile of LiC_{12} is normalized to $\frac{1}{12}$ while that for LiC_6 is normalized to $\frac{1}{6}$. On the same figure, we also show the profile of a single electron populating the π^* bands of graphite taken from Ref. 2 (rigid-band model) and normalized to the same $\frac{1}{12}$ electron. This profile is zero at $q=0$, due to the antisymmetric nature of the wave function of the π^* band with respect to the basal plane. We limit the comparison with the rigid-band model to that of the π^* band, since it has already been demonstrated by the results of the band calculations[9] that bands originating from the lithium $2s$ wave functions are empty in all stages of lithium GIC. Measurements of NMR (Refs. 27 and 28) on LiC_6 also confirm that charge transfer between the intercalant and graphite sheets is close to unity. The small width of the measured difference profile for both stages as compared to that predicted by the rigid-band model, indicates that the additional electron is more delocalized than an electron in the π^* band of graphite, but far more localized than a hypothetical two-dimensional free electron.

It is remarkable that the difference profile for LiC_{12} deviates more for the prediction of a rigid-band model than does LiC_6. Furthermore, when comparing LiC_6 and LiC_{12}, one notices that there is a minimum at $q=0$ in the first stage that does not exist in LiC_{12}. In addition for $q=1.5$ a.u., the difference profile of LiC_{12} shows a noticeable negative region, which is absent in LiC_6. These points will be dealt with in details later.

Figure 3 shows the calculated difference profiles along the c axis for the first two stages. We can see that the major features of the measured spectra are reproduced by theory. The calculated profiles of graphite and LiC_6 are from the work of Chou *et al.*,[2] where the wave functions are obtained using the same procedure[8,9] employed in the present paper for LiC_{12}.

The discrepancy between the total experimental and theoretical profiles, in both directions, is less than 3% of the value at $q=0$. Difference profiles eliminate systemat-

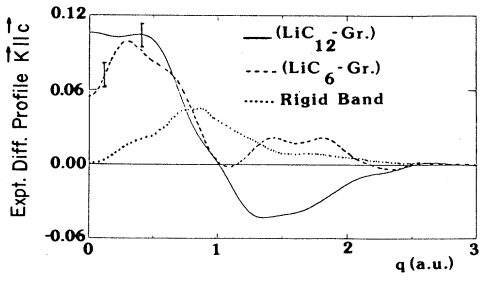

FIG. 2. Difference between measured Compton profiles of Li GIC and graphite for the scattering vector parallel to the c axis: ——, LiC_{12} normalized to $\frac{1}{12}$ electrons; — — —, LiC_6 normalized to $\frac{1}{6}$ electrons; · · · ·, the rigid-band-model prediction, normalized to $\frac{1}{12}$ electrons (Ref. 2).

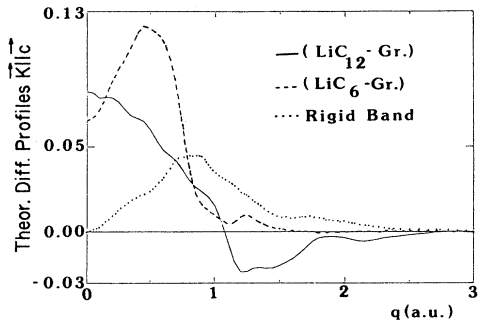

FIG. 3. Difference between calculated Compton profiles of Li GIC and graphite for the scattering vector parallel to the c axis: ——, LiC_{12} normalized to $\frac{1}{12}$ electrons; LiC_6 — — —, normalized to $\frac{1}{6}$ electrons; · · · ·, the rigid-band-model prediction normalized to $\frac{1}{12}$ electrons (Ref. 2). The calculated profiles are convolved with experimental resolution.

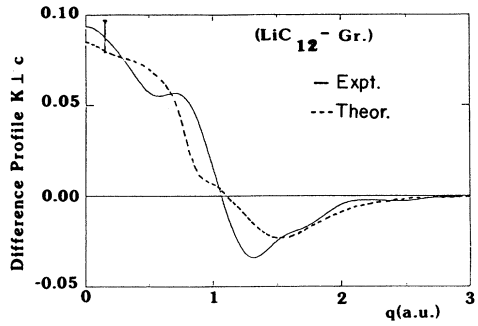

FIG. 5. Difference between the average basal plane Compton profile of LiC_{12} and graphite, normalized to $\frac{1}{12}$ electron: ——, experiment; — — —, theory.

ic errors, both in experiment and theory, including the neglect of correlation effects on the wave functions.[19,29] Thus, in order to further demonstrate the agreement between theory and experiment for LiC_{12}, the calculated and the measured difference profiles are shown in Figs. 4 and 5 for the scattering vector parallel and perpendicular to c axis, respectively. The agreement becomes remarkable if we consider that the maximum discrepancy between the two curves is less than 2% of the value of the DCP at $q=0$. We shall now concentrate on the detailed nature of the difference profile along the c axis.

The difference between the directional Compton profile of GIC and graphite is composed of contributions from a charge originating from the $2s$ electron occupying the π^* bands of graphite, and also from the polarization of a graphite charge due to the presence of the intercalant ion. We have separately calculated these two contributions to the total difference profile for LiC_{12} (Figure 6).

The polarization effect is obtained by calculating the profile due to the σ and π electrons in LiC_{12} and subtracting from it the total profile of graphite as calculated by Chou *et al.*[2] Since this valence difference simply represents the distortion of the filled orbitals of graphite due to the presence of the lithium ions, the net area under this profile difference is zero. The other contribution is due to the electrons occupying the conduction π^* bands in LiC_{12}. Nothing needs to be subtracted from this contribution, due to the fact that these bands are empty in graphite. The area under this contribution, as well as the total, is equal to $\frac{1}{12}$ of an electron, i.e., the extra charge on each carbon atom. The oscillations in the contribution of the conduction electron are due to the variations of the Fermi-surface cross section perpendicular to the scattering vector, i.e., the c axis, as a function of the wave vector in an extended zone scheme, as pointed out by Chou *et al.*[2] The periodicity is equal to the fundamental reciprocal lattice vector along this direction. This effect can be demonstrated by replacing the $C_{n,\mathbf{k}}(\mathbf{r})$ coefficients in the calculation of the Compton profiles by unity. The result is shown in Fig. 7, both for LiC_6 and LiC_{12}. Two important differences should be noted between the two stages. In LiC_{12}, since the lattice constant in the c direction is nearly twice that of LiC_6, the smallest reciprocal-lattice vector in the c direction is almost half that of LiC_6, which explains the ratio of the periodicity in the

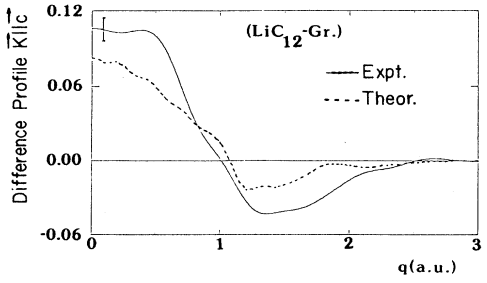

FIG. 4. Difference between the Compton profiles of LiC_{12} and graphite, for the scattering vector parallel to the c axis, normalized to $\frac{1}{12}$ electrons: ——, experiment; — — —, theory.

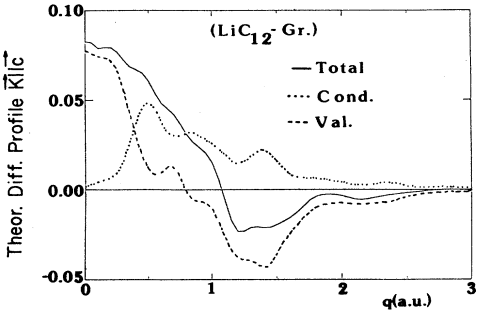

FIG. 6. Decomposition of the calculated difference between the Compton profiles of LiC_{12} and graphite into its valence and conduction contributions. The scattering vector is parallel to the c axis: ——, total difference normalized to $\frac{1}{12}$ electrons; · · · ·, conduction difference normalized to $\frac{1}{12}$ electrons; — — —, valence difference with zero-net area.

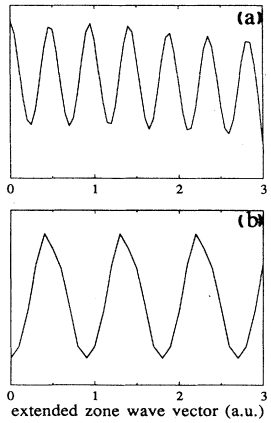

FIG. 7. Variations of the Fermi-surface cross-sectional area perpendicular to the c axis as a function of the extended-zone wave vector: (a) LiC_{12} from the present study, (b) LiC_6 from Ref. 2.

two cases. In addition, our energy-band calculation for LiC_{12} indicates that the cross section of the Fermi surface in the $K-\Gamma-M$ plane of the Brillouin zone is larger than that in the $H-A-L$ plane while the situation is exactly reverse in LiC_6 (Fig. 8). Thus, for LiC_{12} the maxima occur at reciprocal-lattice vectors in this direction, while for LiC_6 the cross section has minimum value at the same vectors. It should be kept in mind that this analysis is only possible for the theoretical results, since it is not possible to decompose the experimental profile into separate contributions of valence polarization and π^* conduction electrons.

We are now in a position to explain the major differences between the spectra of the first- and second-stage compounds. The existence of a peak in the difference profile of LiC_6 at $q=0.5$ a.u. (and the resulting minimum at $q=0$) is due to the large contribution of the conduction electrons which also has a peak at this momentum. However, in LiC_{12} the number of conduction electrons is one-half that of LiC_6, and their smaller

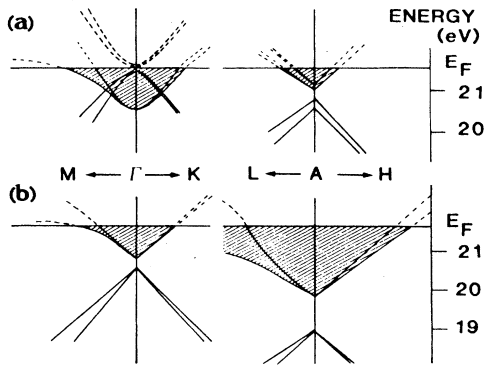

FIG. 8. Schematic representation of the energy bands for lithium GIC in the vicinity of the Fermi level: (a) LiC_{12} from the present study, (b) LiC_6 from Ref. 2.

contribution is masked by the larger effect of polarization. For the same reason, the lack of the negative portion in the LiC_6 difference profile in the neighborhood of $q=1.5$ a.u. is due to the cancellation of the negative contribution of the polarization by the positive value of the conduction-electron profile. This cancellation does not occur in LiC_{12} again since the peak in the conduction-electron contribution occurring in this region is lower than in LiC_6.

The agreement between calculation and experiment for the average basal plane profile (Fig. 5) is equally excellent. The negative part around $q=1.5$ a.u. is present here as well, and is also associated with valence polarization. This negative region, to a lesser degree, can also be observed in the basal plane profile of LiC_6 (Fig. 9 of Ref. 2).

The difference profile demonstrates the importance of the distortion introduced in the graphite electronic distribution due to the presence of the intercalant ions. It is important to point out that such an effect, clearly seen in the theoretical and experimental Compton profiles, actually corresponds to a very small distortion of p_z orbitals, i.e., variations as small as 5×10^{-2} electrons/Å^3 (see Fig. 4 of Ref. 9). Such accuracy is not easily obtained by any means other than Compton scattering. In addition, in approaches such as x-ray diffraction, one needs fairly large single-crystal samples.

IV. CONCLUSION

We have studied the electron-momentum density in the lithium GIC by means of Compton scattering. A new energy-band structure has been calculated for the second-stage compound, LiC_{12} and used to obtain Compton profiles for this compound and compared to those already published for graphite and LiC_6. We have confirmed the inapplicability of the rigid-band model to LiC_{12}. The agreement between theory and experiment for LiC_{12} is remarkable as was previously shown for graphite and LiC_6. When comparing the difference profiles for LiC_6 and LiC_{12}, it appears that the deviation from the rigid-band model is larger in the second than in the first stage. This surprising result is due to the relative sizes of the two contributions to the difference profile. One contribution is from polarization of the valence density of graphite due to the presence of the intercalant ion and is of comparable magnitude in both stages. The second and compensating contribution is due to the conduction electrons occupying the π^* bands. Since their number per carbon atom is half as many in LiC_{12} as in LiC_6 the difference density in the former reflects more the polarization contribution, i.e., the non-rigid-band effects. Thus this study, which is performed in the momentum space, allows one to probe variations in electron density which are very small in magnitude: this turns out to be a great advantage of this method.

ACKNOWLEDGMENTS

The authors would like to express their gratitude to Dr. Daniel Guérard for providing the samples used in the measurements and for valuable discussions.

*Also at Laboratoire pour l'Utilisation du Rayonnement Electromagnétique, Bâtiment 209D, Université de Paris–Sud, 91405 Orsay CEDEX, France.

[1]M. S. Dresselhaus and G. Dresselhaus, Adv. Phys. **30**, 139 (1981).
[2]M. Y. Chou, S. G. Louie, M. L. Cohen, and N. A. W. Holzwarth, Phys. Rev. B **30**, 1062 (1984).
[3]M. Y. Chou, Marvin L. Cohen, and S. G. Louie, Phys. Rev. B **33**, 6619 (1986).
[4]G. Loupias, J. Chomilier, and D. Guérard, J. Phys. (Paris) Lett. **45**, L301 (1984).
[5]G. Loupias, J. Chomilier, and D. Guérard, Solid State Commun. **55**, 299 (1985).
[6]S. Basu, C. Zeller, P. Flanders, C. D. Fuerst, W. D. Johnson, and J. E. Fischer, Mater. Sci. Eng. **38**, 275 (1979).
[7]E. McRae, D. Billaud, J. F. Maréché, and A. Hérold, Physica B+C **99B**, 489 (1980).
[8]N. A. W. Holzwarth, S. G Louie, and S Rabii, Phys. Phys Rev B **26**, 5382 (1982).
[9]N. A. W. Holzwarth, S. G. Louie, and S. Rabii, Phys. Rev. B **28**, 1013 (1983).
[10]L. Samuelson and I. P. Batra, J. Phys. C **13**, 5105 (1980).
[11]R. V. Kasowski, Phys. Rev. B **25**, 4189 (1982).
[12]M. Posternak, A. Baldereschi, A. J. Freeman, E. Wimmer, and M. Weinert, Phys. Rev. Lett **50**, 761 (1983).
[13]D. Guérard (private communication).
[14]D. Guérard and A. Hérold, Carbon **13**, 337 (1975).
[15]J. W. M. DuMond, Phys. Rev. **33**, 643 (1929); **36**, 146 (1930).
[16]P. Eisenberger and P. M. Platzman, Phys. Rev. A **2**, 415 (1970).
[17]A. Issolah, B. Lévy, A. Beswick, and G. Loupias, Phys. Rev. A **38**, 4509 (1988).
[18]P. Rennert, Th. Dorre, and U. Glaser, Phys. Status Solidi B **87**, 221 (1978).
[19]P. Rennert Phys. Status Solidi B **105**, 567 (1981).
[20]P. Hohenberg and W. Kohn, Phys. Rev. **136**, B864 (1964).
[21]W. Kohn and L. J. Sham, Phys. Rev. **140**, A1133 (1965).
[22]D. R. Hamann, M. Schlüter, and C. Chiang, Phys. Rev. Lett. **43**, 1494 (1979).
[23]L. Hedin and B. I. Lundqvist, J. Phys. C **4**, 2064 (1971).
[24]S. G. Louie, K. M. Ho, and M L Cohen, Phys. Rev. B **19**, 1774 (1979).
[25]G. Loupias, J. Petiau, A. Issolah, and M. Schneider, Phys. Status Solidi B **102**, 79 (1980).
[26]J. Chomilier, G. Loupias, and J. Felsteiner, Nucl. Instrum. Methods A **235**, 603 (1985).
[27]H. Estrade, J. Conard, P. Lauginie, P. Heitjons, F. Fujara, W. Butler, G. Kiese, H. Ackermann, and D. Guérard, Physica B+C **99B**, 531 (1980).
[28]P. Lauginie, Synth. Met. **23**, 311 (1988).
[29]M. L. Chou, P. K. Lam, M. L Cohen, G. Loupias, J. Chomilier, and J. Petiau, Phys. Rev. Lett. **49**, 1452 (1982).